Heliyon 10 (2024) e26611

Contents lists available at ScienceDirect

Heliyon

journal homepage: www.cell.com/heliyon

Research article

Mathematical modeling and stability analysis of the novel fractional model in the Caputo derivative operator: A case study

Rania Saadeh [a,*], Mohamed A. Abdoon [b], Ahmad Qazza [a], Mohammed Berir [c], Fathelrhman EL Guma [c,d], Naseam Al-kuleab [e], Abdoelnaser M Degoot [f]

[a] Department of Mathematics, Zarqa University, Zarqa 13110, Jordan
[b] Department of Basic Sciences, Common First Year Deanship, King Saud University, Riyadh 12373, Saudi Arabia
[c] Department of mathematics, Faculty of Science and Arts, Al baha university, Baljurashi 65622, Saudi Arabia
[d] Department of statistical Study, Peace University, Sudan
[e] Department of Mathematics and Statistics, College of Science, King Faisal University, Al-Ahsa 31982, Saudi Arabia
[f] African institute for Mathematical Sciences, Kigali, Rwanda

ARTICLE INFO

Keywords:
Fractional model
Visceral leishmaniasis
Disease transmission
Stability analysis
Caputo fractional derivative
Simulation

ABSTRACT

The fundamental goal of this research is to suggest a novel mathematical operator for modeling visceral leishmaniasis, specifically the Caputo fractional-order derivative. By utilizing the Fractional Euler Method, we were able to simulate the dynamics of the fractional visceral leishmaniasis model, evaluate the stability of the equilibrium point, and devise a treatment strategy for the disease. The endemic and disease-free equilibrium points are studied as symmetrical components of the proposed dynamical model, together with their stabilities. It was shown that the fractional calculus model was more accurate in representing the situation under investigation than the classical framework at $\alpha = 0.99$ and $\alpha = 0.98$. We provide justification for the usage of fractional models in mathematical modeling by comparing results to real-world data and finding that the new fractional formalism more accurately mimics reality than did the classical framework. Additional research in the future into the fractional model and the impact of vaccinations and medications is necessary to discover the most effective methods of disease control.

1. Introduction

The utilization of models of illnesses is of utmost importance as it facilitates the comprehension of their dynamics, enables the prediction of their propagation, and aids in the development of efficient management measures [1]. Through the utilization of mathematical equations, researchers are able to get valuable insights into the complex interplay between hosts, infections, and environmental factors, which may not be readily discernible through empirical data alone. These models facilitate the elucidation of the fundamental mechanisms of disease transmission, assessment of the effectiveness of therapies, and examination of various hypothetical situations. Nevertheless, the resolution of these intricate mathematical equations frequently necessitates the utilization of numerical techniques owing to the arduousness associated with acquiring analytical answers. Numerical methodologies such as

* Corresponding author.
E-mail address: rsaadeh@zu.edu.jo (R. Saadeh).

https://doi.org/10.1016/j.heliyon.2024.e26611
Received 19 August 2023; Received in revised form 2 February 2024; Accepted 15 February 2024

Available online 23 February 2024

numerical methods [2,3], Laplace residual power series [4], facilitate the estimation of solutions, the simulation of illness trajectories, and the evaluation of the implications of diverse intervention options for researchers. The integration of mathematical modeling and numerical approaches provides us with the capability to make well-informed judgments, effectively control outbreaks, and eventually ensure the protection of public health on a worldwide level.

Leishmaniasis is a neglected parasitic illness that affects 97 nations in the Americas, Africa, Asia, and Europe. More than 20 different species of Leishmania are the primary causes of the disease, and infected female phlebotomine sand flies bite people to spread the disease. The three primary leishmaniasis clinical manifestations are caused by different species of the Leishmania donovani complex: cutaneous (CL), mucocutaneous (MCL), and visceral (VL) [5].

Leishmaniasis is a neglected parasitic illness that affects 97 nations in America, Africa, Asia, and Europe. More than 20 different species of Leishmania are the primary cause of the disease, and infected female phlebotomine sand flies bite people to spread the disease. Various species of the Leishmania donovani complex cause the three main clinical presentations of leishmaniasis: cutaneous (CL), mucocutaneous (MCL), and visceral (VL) [5].

The parasite that causes VL in Sudan is a member of the Leishmania donovani sensulato cluster. Leishmania archibaldi and Leishmania infantum have been isolated from people and canines in Gedaref state, eastern Sudan. Leishmania major zymodeme LON-1 is a parasite that causes CL in Sudan [6]. Increased population movement associated with armed conflicts, as well as exposure to sandfly vectors, has contributed to the disease's expansion into previously non-endemic areas of East Africa [7–9]. India, Bangladesh, Sudan, South Sudan, Brazil, and Ethiopia account for more than 90% of all cases of visceral leishmaniasis (VL) worldwide, accounting for between 20,000 and 40,000 fatalities annually [9]. Sudan has three main locations where VL is common: the east, center, and south. There are also a few places where it happens occasionally, such as Kordofan State and the central and western parts of Darfur State [10].

Many mathematical models of VL transmission dynamics have been developed in recent years (e.g., [11,12]), revolving around people, reservoirs, and sandflies. Song et al. [13] fitted a VL model to cumulative cases from 2004 to 2016 for the epidemic in Kashgar and found that it was very likely that the cumulative incidence of kalaazar would increase in Kashgar. Similarly, the fundamental replicability index is calculated. Sensitivity analysis showed that decreasing the amount of time sandflies spent around dogs was an efficient strategy for decreasing the prevalence of kala-azar. To study the dynamics of visceral leishmaniasis in Sudan, Elmojtaba et al. [14]constructed a mathematical model that considers three groups, analyzed the equilibrium point and its stability, and provided a foundation for the control and eventual eradication of the illness. To acquire threshold conditions and provide numerical simulation results, Sinan et al. [15] presented a mathematical analysis of a cutaneous leishmaniasis disease model that includes properties such as positivity, equilibrium points, and reproductive number. Local and global stability analyses of the equilibrium points were also performed using the Lyapunov function method and the third additive compound matrix technique. Sensitivity analysis was also performed using a nonstandard finite-difference scheme. Many researchers, both from old research and modern research, dealt with this topic with fractional models [16–18].

The main objective of this study is to propose a new mathematical operator, the Caputo fractional-order derivative operator, for modeling leishmaniasis. The fractional Euler approach was successfully used to simulate the dynamics of a new fractional visceral leishmaniasis model. The fractional visceral leishmaniasis model outperformed the traditional model, according to numerical comparisons with actual data from Gedaref State in eastern Sudan.

The use of Caputo fractional derivatives in disease modeling is a promising avenue for future research. It can offer more accurate and nuanced insights into disease dynamics, which can be invaluable in improving disease control and management strategies. As the field of fractional calculus and epidemiology continues to evolve, it's likely that more innovative applications and approaches will emerge [19–22].

This paper consists of the following sections: section 2, model construction, section 3, parameter estimate, section 4, model analysis, section 5, fractional Euler method, section 6, numerical simulation The final conclusion of this paper is provided.

2. Model construction

This section describes VL dynamics by using modified SEIR model. The model comprises three distinct populations: reservoirs, vectors, and human beings. The entire human population (N_h^*) is partitioned into six sub-populations: exposed (E_h^*), susceptible (S_h^*), detected infected (I_d^*), undetected infected (I_u^*), PKDL-infected (P_h^*), and recovered individuals (R_h^*). The total vector population N_v^* is split into two sub-populations, similar to how the reservoir population is split into susceptible S_r^* reservoirs and infected reservoirs I_r^*:

$$N_h^*(t) = S_h^*(t) + E_h^*(t) + I_d^*(t) + I_u^*(t) + P_h^*(t) + R_h^*(t),$$
$$N_v^*(t) = S_v^*(t) + I_v^*(t),$$
$$N_r^*(t) = S_r^*(t) + I_r^*(t).$$

Initially, the parasite infects human, vector, and reservoir populations, which with constant birth rates λ_h^*, λ_v^* and λ_r^* and die naturally at μ_h^*, μ_v^*, and μ_r^* The parasite infects susceptible people with $f_1 = \beta_1^* \frac{I_v(t)}{N_h(t)}(1 - \alpha_h^*(t))$, where β_1^* is vector-borne infection probability and $\alpha_h^*(t) \in [0, 1]$ Effective non-pharmaceutical human population protection strategies include treated bed-nets. If interventions were 100% effective $\alpha_h^*(t) = 1$, no new VL cases would occur.

Individuals in E_h^* survive for $\frac{1}{\omega^*}$ days before dying naturally at μ_h, becoming infectious at I_d^* at $\epsilon^*(t)$, or undetected at $1-\epsilon^*(t)$. At time t, the parameter $epsilon^*(t)$ measures the effectiveness of focused surveillance actions for case detection, such as capacity development and early diagnosis. Without monitoring, all infected would go unnoticed. Individuals in I_d^* compartment get therapy, recover at σ_1^*, acquire PKDL at ρ_1^*, or die at δ_1^* and μ_h^* owing to VL infection and natural causes, respectively.

Surveillance systems do not record or treat I_u^*. However, these individuals recover naturally at γ_1^* due to immunity, acquire PKDL at ρ_2^*, and die at δ_2^* and μ_h^* due to VL infection and natural mortality, respectively. Asymptomatic, sub-clinical, and health program-covered individuals are in I_u^*. Ph class individuals, P_h^*, recover naturally and treatment-induced at rates of σ_2^* and γ_2^*, respectively, and die naturally at rate μ_h^*. R_h^*, individuals die naturally at μ_h^* and face re-exposure at η^* due to reduced VL-induced immunity. $(S_v^*(t))$ contract VL from infected vectors $f_2=\beta_1^*\frac{I_v(t)}{N_r^*(t))}$, and are reduced by the effectiveness of methods used to reduce the reservoir population, like euthanizing diseased animals and vaccinating dogs. The transmission probability from an infected vector $(beta_1^*)$ is considered to be the same for susceptible persons and reservoirs. Host stage determines the likelihood of VL transmission from infected to vector [23]. We use parameters $beta_2^*, beta_3^*, beta_4^*$, and $beta_5^*$ to indicate transmission probability per discovered, undetected, PKDL, and infected reservoir. The vector population's overall infection force is

$$f_3=\left(\left(\beta_2^*\frac{I_d^*(t)}{N_h^*(t)}+\beta_3^*\frac{I_u^*(t)}{N_h^*(t)}+\beta_4^*\frac{P_h^*(t)}{N_h^*(t)}\right)(1-\alpha_h^*(t))+\beta_5^*\frac{I_r^*(t)}{N_r^*(t)}\right)S_v^*(t).$$

$(S_v^*(t))$ further lowered by $\alpha_v^*(t)$, which reflects the effectiveness of vector control efforts like pesticide spraying. The differential equations in System 1 quantify the VL transmission dynamic, as shown in 1.

$$\begin{aligned}
S_h^{*\prime}(t)&=\lambda_h^*-\beta_1^*I_v^*(t)((1-\alpha_h^*(t))\frac{S_h^*(t)}{N_h^*(t)}+\eta R_h^*(t)-\mu_h^*S_h^*(t),\\
E_h^{*\prime}(t)&=\beta_1^*I_v^*(t)((1-\alpha_h^*(t))\frac{S_h^*(t)}{N_h^*(t)}-(\omega^*+\mu_h^*)E_h^*(t),\\
I_d^{*\prime}(t)&=\epsilon^*(t)\omega^*E_h^*(t)-\left(\sigma_1^*+\rho_1^*+\delta_1^*+\mu_h^*\right)I_d^*(t),\\
I_u^{*\prime}(t)&=\omega^*\left[1-\epsilon^*(t)\right]E_h^*(t)-\left(\mu_h^*+\delta_2^*+\rho_2^*+\gamma_1^*\right)I_u^*(t),\\
P_h^{*\prime}(t)&=\rho_1^*I_d^*(t)+\rho_2^*I_u^*(t)-(\sigma_2^*+\gamma_2^*+\mu_h^*)P_h^*(t),\\
R_h^{*\prime}(t)&=\sigma_1^*I_d^*(t)+\gamma_1^*I_u^*(t)+(\sigma_2^*+\gamma_2^*)P_h^*(t)-(\eta^*+\mu_h^*)R_h^*(t),\\
S_r^{*\prime}(t)&=\lambda_r^*-\beta_1^*I_v^*(t)\frac{S_r^*(t)}{N_r^*(t)}-(\alpha_r^*(t)+\mu_r^*)S_r^*(t),\\
I_r^{*\prime}(t)&=\beta_1^*I_v^*(t)\frac{S_r^*(t)}{N_r^*(t)}-(\alpha_r^*(t)+\mu_r^*)I_r^*(t),\\
S_v^{*\prime}(t)&=-\left(\left(\beta_2^*\frac{I_d^*(t)}{N_h^*(t)}+\beta_3^*\frac{I_u^*(t)}{N_h^*(t)}+\beta_4^*\frac{P_h^*(t)}{N_h^*(t)}\right)(1-\alpha_h^*(t))+\beta_5^*\frac{I_r^*(t)}{N_r^*(t)}\right)S_v^*(t)\\
&\quad+\lambda_v^*-(\alpha_v^*(t)+\mu_v^*)S_v^*(t),\\
I_v^{*\prime}(t)&=\left(\left(\beta_2^*\frac{I_d^*(t)}{N_h^*(t)}+\beta_3^*\frac{I_u^*(t)}{N_h^*(t)}+\beta_4^*\frac{P_h^*(t)}{N_h^*(t)}\right)(1-\alpha_h^*(t))+\beta_5^*\frac{I_r^*(t)}{N_r^*(t)}\right)S_v^*(t)\\
&\quad-(\alpha_v^*(t)+\mu_v^*)I_v^*(t).
\end{aligned}\tag{1}$$

The model's formulation implicitly contains the following three equations:

$$\begin{aligned}
N_h^{\prime *}(t)&=\lambda_h^*-\mu_h^*N_h^*(t)-\delta_1^*I_d^*(t)-\delta_2^*I_u^*(t),\\
N_r^{\prime *}(t)&=\lambda_r^*-(\alpha_r^*(t)+\mu_r^*)N_r^*(t),\\
N_v^{\prime *}(t)&=\lambda_v^*-(\alpha_v^*(t)+\mu_v^*)N_v^*(t).
\end{aligned}\tag{2}$$

In system (1), every parameter, beginning value, and compartment is non-negative. In section 4, Here are several tables with model parameters and values. The proposed VL transmission model includes variables, parameters, transition rates, and infection forces for human, reservoir, and vector populations (Fig. 1).

2.1. Mathematical analysis

In system (2), the disease-free state ($\delta_1^*=\delta_2^*=0$) and long-term population ($t\to\infty$) are defined by natural growth and death rates, $N_h^*=\frac{\lambda_h^*}{\mu_h^*}$. Malaria programmes use pesticide spraying to reduce reservoir and vector populations, which may continue after VL

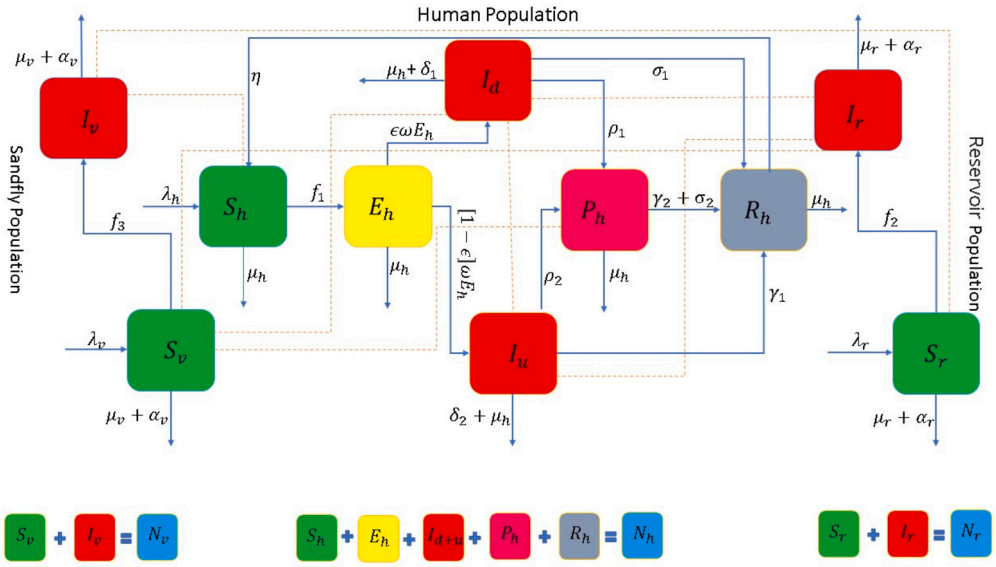

Fig. 1. Diagram of the proposed VL transmission model.

is eradicated. Consequently, natural causes and interventions determine reservoir and vector populations. We know of no other programme for regulating animal populations in the region of concern. It is appropriate to set $\alpha_r^* = 0$, even though mathematical analysis allows for certain differences. In the long term, $N_r^* = \dfrac{\lambda_r^*}{\mu_r^*}$ and $N_v^* = \dfrac{\lambda_v^*}{\alpha_v^* + \mu_v^*}$ represents the disease-free equilibrium coordinates of system (1), represented by E^0.

$$E^0 = \left(\frac{\lambda_h^*}{\mu_h^*}, 0, 0, 0, 0, 0, \frac{\lambda_r^*}{\mu_r^*}, 0, \frac{\lambda_v^*}{\alpha_v^* + \mu_v^*}, 0\right).$$

Since system (1) figures out the number of live things, l there is a logica area in which to examine it is

$$\Omega = \left\{\left(I_v^*, S_v^*, I_r^*, S_r^*, R_h^*, P_h^*, I_u^*, I_d^*, E_h^*, S_h^*,\right) \in \mathbb{R}_+^{10} : I_u^* + I_d^* + E_h^* + S_h^* + R_h^* + P_h^* \le N_h^*(0),\ I_r^* + S_r^* \le N_r^*(0),\ I_v^* + S_v^* \le N_v^*(0)\right\}$$

which is a limited, positively-invariant domain for model (1) and has non-negative initial conditions in $\mathbb{R}_+^{10}$ (see Section 4.2. $\mathcal{R}_0$ (The reproduction number) of model (1) was calculated using the next generation operator [24] according to Equation (7). In Section 4.2, we demonstrated the disease-free equilibrium and system stability using $\mathcal{R}_0$.

3. Fractional-order model

In this section, we discuss The Fractional VL model and the one described above using the ten differential equations in system (3), and Table 1 provides descriptions, values, and ranges for all model parameters. Fractional models are memory-based systems; therefore, they have requirements and tools to describe them. Researchers in the fields of biology, physics, and engineering have found that fractional-order models can yield more accurate predictions of experimental outcomes than their integer-order counterparts [25,26,1,27]. Due to this crucial property, Models of fractional order are suitable for the dynamical systems that are being studied. One of these tools is Caputo operator, the focus in this research is on the Caputo fractional derivative because this derivative has a property because it is accurate in describing the dynamics of the disease, the following nonlinear system stands in for the Caputo fractional-order model:

$$\begin{aligned}
{}_0^C D S_h^*(t) &= \lambda_h^* - \beta_1^* I_v^*(t)((1-\alpha_h^*(t))\frac{S_h^*(t)}{N_h^*(t)} + \eta R_h^*(t) - \mu_h^* S_h^*(t),\\
{}_0^C D E_h^*(t) &= \beta_1^* I_v^*(t)((1-\alpha_h^*(t))\frac{S_h^*(t)}{N_h^*(t)} - (\omega^* + \mu_h^*)E_h^*(t),\\
{}_0^C D I_d^*(t) &= \epsilon^*(t)\omega^* E_h^*(t) - \left(\sigma_1^* + \rho_1^* + \delta_1^* + \mu_h^*\right) I_d^*(t),\\
{}_0^C D I_u^*(t) &= \omega^* \left[1 - \epsilon^*(t)\right] E_h^*(t) - \left(\mu_h^* + \delta_2^* + \rho_2^* + \gamma_1^*\right) I_u^*(t),\\
{}_0^C D P_h^*(t) &= \rho_1^* I_d^*(t) + \rho_2^* I_u^*(t) - (\sigma_2^* + \gamma_2^* + \mu_h^*)P_h^*(t),\\
{}_0^C D R_h^*(t) &= \sigma_1^* I_d^*(t) + \gamma_1^* I_u^*(t) + (\sigma_2^* + \gamma_2^*)P_h^*(t) - (\eta^* + \mu_h^*)R_h^*(t),
\end{aligned} \tag{3}$$

$$
\begin{aligned}
{}_0^C D S_r^*(t) &= \lambda_r^* - \beta_1^* I_v^*(t)\frac{S_r^*(t)}{N_r^*(t)} - (\alpha_r^*(t) + \mu_r^*)S_r^*(t),\\
{}_0^C D I_r^*(t) &= \beta_1^* I_v^*(t)\frac{S_r^*(t)}{N_r^*(t)} - (\alpha_r^*(t) + \mu_r^*)I_r^*(t),\\
{}_0^C D S_v^*(t) &= -\left(\left(\beta_2^*\frac{I_d^*(t)}{N_h^*(t)} + \beta_3^*\frac{I_u^*(t)}{N_h^*(t)} + \beta_4^*\frac{P_h^*(t)}{N_h^*(t)}\right)(1-\alpha_h^*(t)) + \beta_5^*\frac{I_r^*(t)}{N_r^*(t)}\right)S_v^*(t)\\
&\quad + \lambda_v^* - (\alpha_v^*(t) + \mu_v^*)S_v^*(t),\\
{}_0^C D I_v^*(t) &= \left(\left(\beta_2^*\frac{I_d^*(t)}{N_h^*(t)} + \beta_3^*\frac{I_u^*(t)}{N_h^*(t)} + \beta_4^*\frac{P_h^*(t)}{N_h^*(t)}\right)(1-\alpha_h^*(t)) + \beta_5^*\frac{I_r^*(t)}{N_r^*(t)}\right)S_v^*(t)\\
&\quad - (\alpha_v^*(t) + \mu_v^*)I_v^*(t).
\end{aligned}
$$

Where ${}_0^C D(.)$, is the Caputo fractional derivative.

Definition 1: ([[28]]). The fractional-order derivative of a function $f(t)$ based upon the Caputo definition with order $\alpha > 0$ is given by

$$
{}^c D_{0,t}^{\alpha}(f(t)) = \frac{1}{\Gamma(m-\alpha)}\int_0^t (t-s)^{m-\alpha-1} f^{(m)}(s)ds, t > 0,
$$

where $m-1 < \alpha \le m, m \in \mathbb{N}$.

4. Analysis of the VL model

We want to analyze the dynamic aspects of the VL disease model in this part. (1) in the primary text, which measures the extinction or spread of illness within a population.

4.1. Boundedness and positivism

Theorem 1. *(positivity) The matching solution set will exist if the beginning conditions are non-negative.*

$$
\left(I_v^*(t), S_v^*(t), I_r^*(t), S_r^*(t), R_h^*(t), P_h^*(t), I_u^*(t), I_d^*(t), E_h^*(t), S_h^*(t)\right),
$$

of system (1) *is non-negative for all* $t > 0$. *Moreover,*

$$
\lim_{t\to\infty} N_v^*(t) \le N_v^*(0), \lim_{t\to\infty} N_r^*(t) \le N_r^*(0), \lim_{t\to\infty} N_h^*(t) \le N_h^*(0)
$$

and the region

$$
\begin{aligned}
\Omega = \Big\{&\left(I_v^*, S_v^*, I_r^*, S_r^*, R_h^*, P_h^*, I_u^*, I_d^*, E_h^*, S_h^*\right) \in \mathbb{R}_+^{10} :\\
&S_h^* + E_h^* + I_d^* + I_u^* + P_h^* + R_h^* \le N_h^*(0), S_r^* + I_r^* \le N_r^*(0), S_v^* + I_v^* \le N_v^*(0)\Big\},
\end{aligned}
$$

is positively-invariant for the model (1) *any non-negative initial conditions in* $\mathbb{R}_+^{10}$.

Since all equations and initial conditions are non-negative Proposition and You can refer to the proof of the theorem in [29], we can conclude that $S_h^*(t) \ge 0, E_h^*(t) \ge 0, I_d^*(t) \ge 0, I_u^*(t) \ge 0, P_h^*(t) \ge 0, R_h^*(t) \ge 0, S_r^*(t) \ge 0, I_r^*(t) \ge 0, S_v^*(t) \ge 0$, and $I_v^*(t) \ge 0$, for all $t > 0$.

4.2. The fundamental number for reproduction

$\mathcal{R}_0$ represents the fundamental reproduction number, which is the expected value of the secondary infection rate per time unit. E_h^*, I_d^*, I_u^*, P_h^*, I_r^*, and I_v^* are the six infected classes in system (1). Consequently, system (1) is simplified to the new system that follows:

$$
\begin{aligned}
E_h^{*\prime}(t) &= \beta_1^* I_v^*(t)((1-\alpha_h^*(t))\frac{S_h^*(t)}{N_h^*(t)} - (\omega^* + \mu_h^*)E_h^*(t),\\
I_d^{*\prime}(t) &= \epsilon^*(t)\omega^* E_h^*(t) - \left(\sigma_1^* + \rho_1^* + \delta_1^* + \mu_h^*\right) I_d^*(t),\\
I_u^{*\prime}(t) &= \omega^* \left[1-\epsilon^*(t)\right] E_h^*(t) - \left(\mu_h^* + \delta_2^* + \rho_2^* + \gamma_1^*\right) I_u^*(t),\\
P_h^{*\prime}(t) &= \rho_1^* I_d^*(t) + \rho_2^* I_u^*(t) - (\sigma_2^* + \gamma_2^* + \mu_h^*)P_h^*(t),\\
I_r^{*\prime}(t) &= \beta_1^* I_v^*(t)\frac{S_r^*(t)}{N_r^*(t)} - (\alpha_r^*(t) + \mu_r^*)I_r^*(t),\\
I_v^{*\prime}(t) &= \left(\left(\beta_2^*\frac{I_d^*(t)}{N_h^*(t)} + \beta_3^*\frac{I_u^*(t)}{N_h^*(t)} + \beta_4^*\frac{P_h^*(t)}{N_h^*(t)}\right)(1-\alpha_h^*(t)) + \beta_5^*\frac{I_r^*(t)}{N_r^*(t)}\right) S_v^*(t)\\
&\quad - (\alpha_v^*(t) + \mu_v^*)I_v^*(t).
\end{aligned}
\tag{4}
$$

The average detection rate $\epsilon^*(t)$ is assumed to be constant for non-pharmaceutical interventions $\alpha_h^*(t) = \alpha_h^*$, reservoir control interventions $\alpha_h^*(t) = \alpha_h^*$, and vector control interventions $\alpha_h^*(t) = \alpha_h^*$. Rewrite system (4) in vector form [30].

$$\frac{dx}{dt} = f(x) = \mathcal{F}(x) - \mathcal{V}(x),$$

where

$$
\mathcal{F}(x) = \begin{bmatrix}
\frac{\beta_1^* I_v^* S_h^*\left(1-\alpha_h^*\right)}{N_h^*}\\
0\\
0\\
0\\
\frac{\beta_1^* I_v^* S_r^*}{N_r^*}\\
\left[\left(\frac{\beta_2^* I_d^*}{N_h^*} + \frac{\beta_3^* I_u^*}{N_h^*} + \frac{\beta_4^* P_h^*}{N_h^*}\right)\left(1-\alpha_h^*\right) + \frac{\beta_5^* I_r^*}{N_r^*}\right] S_v^*
\end{bmatrix},
$$

and $\mathcal{V}(x) = \mathcal{V}^-(x) - \mathcal{V}^+(x)$ such that

$$
\mathcal{V}^+(x) = \begin{bmatrix}
0\\
\epsilon^*\omega^* E_h^*\\
(1-\epsilon^*)\omega^* E_h^*\\
\rho_1^* I_d^* + \rho_2^* I_u^*\\
0\\
0
\end{bmatrix} \quad \text{and} \quad
\mathcal{V}^-(x) = \begin{bmatrix}
\left(\omega^* + \mu_h^*\right) E_h^*\\
\left(\sigma_1^* + \rho_1^* + \delta_1^* + \mu_h^*\right) I_d^*\\
\left(\gamma_1^* + \rho_2^* + \delta_2^* + \mu_h^*\right) I_u^*\\
\left(\gamma_2^* + \sigma_2^* + \mu_h^*\right) P_h^*\\
\left(\alpha_r^* + \mu_r^*\right) I_r^*\\
\left(\alpha_v^* + \mu_v^*\right) I_v^*
\end{bmatrix}.
$$

We can confirm that the requirements (A1)–(A5) in [24] are met by system (4). It is simple to determine that from the aforementioned functions that: (A1) $\mathcal{F}_i(x)$, $\mathcal{V}_i^+(x)$, and $\mathcal{V}_i^-(x) \geq 0$, for $i = 1,2,3,4,5,6$. This is because $x_i \geq 0$. Therefore, all of the compartments are non-negative since they involve directed transfers of living things; keep in mind that ϵ^* and $\alpha \in [0,1]$.
(A2) then $\mathcal{V}_i^-(x) = 0$, if $x_i = 0$, for $i = 1,2,3,4,5,6$. i.e., the elimination of living things does not occur from a compartment that is empty.
(A3) $\mathcal{F}_i = 0$ for $i \notin \{1,2,3,4,5,6\}$. i.e., the incidence of infection for uninfected compartments (S_h, R_h, S_r, and S_v) is zero, see the main text.
(A4) then $\mathcal{F}_i(x) = 0$ and $\mathcal{V}_i^+(x) = 0$, if $x \in E^0$, for $i = 1,2,3,4,5,6$.
(A5) if $\mathcal{F}(x) = 0$, then the Jacobian matrix of system (4) is given by

$$
Df(x_0) = \begin{bmatrix}
-(\omega^*+\mu_h^*) & 0 & 0 & 0 & 0 & 0\\
\epsilon^*\omega^* & -(\sigma_1^*+\rho_1^*+\delta_1^*+\mu_h^*) & 0 & 0 & 0 & 0\\
(1-\epsilon^*)\omega^* & 0 & -(\gamma_1^*+\rho_2^*+\delta_2^*+\mu_h^*) & 0 & 0 & 0\\
0 & \rho_1^* & \rho_2^* & -(\gamma_2^*+\sigma_2^*+\mu_h^*) & 0 & 0\\
0 & 0 & 0 & 0 & -(\alpha_r^*+\mu_r^*) & 0\\
0 & 0 & 0 & 0 & 0 & -(\alpha_v^*+\mu_v^*)
\end{bmatrix}.
$$

The eigenvalues of $Df(x_0)$ are: $-(\omega^* + \mu_h^*), -(\sigma_1^* + \rho_1^* + \delta_1^* + \mu_h^*), -(\gamma_1^* + \rho_2^* + \delta_2^* + \mu_h^*), -(\gamma_2^* + \sigma_2^* + \delta_3^* + \mu_h^*), -(\alpha_r^* + \mu_r^*)$, and $-(\alpha_v^* + \mu_v^*)$, and each one has negative real part given by

$$F=\begin{bmatrix} 0 & 0 & 0 & 0 & 0 & \beta_1^*\left(1-\alpha_h^*\right) \\ 0 & 0 & 0 & 0 & 0 & 0 \\ 0 & 0 & 0 & 0 & 0 & 0 \\ 0 & 0 & 0 & 0 & 0 & 0 \\ 0 & 0 & 0 & 0 & 0 & \beta_1^* \\ 0 & \beta_2^*K_1 & \beta_3^*K_1 & \beta_4^*K_1 & \beta_5^*K_2 & 0 \end{bmatrix}, \tag{5}$$

where $K_1=\frac{(1-\alpha_h^*)\mu_v^*N_v}{(\alpha_v^*+\mu_v^*)N_h^*}$, and $K_2=\frac{\mu_v^*N_v^*}{(\alpha_v^*+\mu_v^*)N_r^*}$.

$$V=\begin{bmatrix} (\omega^*+\mu_h^*) & 0 & 0 & 0 & 0 & 0 \\ -\epsilon^*\omega^* & \sigma_1^*+\rho_1^*+\delta_1^*+\mu_h^* & 0 & 0 & 0 & 0 \\ -\left(1-\epsilon^*\right)\omega^* & 0 & \gamma_1^*+\rho_2^*+\delta_2^*+\mu_h^* & 0 & 0 & 0 \\ 0 & -\rho_1^* & -\rho_2^* & \gamma_2^*+\sigma_2^*+\mu_h^* & 0 & 0 \\ 0 & 0 & 0 & 0 & \alpha_r^*+\mu_r^* & 0 \\ 0 & 0 & 0 & 0 & 0 & \alpha_v^*+\mu_v^* \end{bmatrix}. \tag{6}$$

Equations (5) and (6) yield the reproduction number of the system (2), $\mathcal{R}_0$, is given by equation (7)

$$\mathcal{R}_0=\rho^*(FV^{-1}). \tag{7}$$

Letting

$$A_1=\sigma_1^*+\rho_1^*+\delta_1^*+\mu_h^*,\quad A_2=\gamma_1^*+\rho_2^*+\delta_2^*+\mu_h^*,\quad A_3=\gamma_2^*+\sigma_2^*+\mu_h^*.$$

Thus

$$\mathcal{R}_0=\sqrt{\frac{\beta_1^*\left(K_1\omega^*(1-\alpha_h^*)(\alpha_r^*+\mu_r^*)\left(A_1(1-\epsilon^*)(A_3\beta_3^*+\beta_4^*\rho_2^*)+\epsilon^*A_2(A_3\beta_2^*+B_4\rho_1^*)\right)+K_2(\omega^*+\mu_h^*)A_1A_2A_3\beta_5^*\right)}{A_1A_2A_3(\omega^*+\mu_h^*)(\mu_v^*+\alpha_v^*)(\mu_r^*+\alpha_r^*)}}.$$

4.3. Stability analysis of the model

Theorem 2. *System* (1) *at disease-free equilibrium point* E_{dfe} *is locally asymptotically stable if* $\mathcal{R}_0<1$ *and unstable if* $\mathcal{R}_0>1$.

Proof. Regarding the system of equation (1), the Jacobian matrix [24] Equation (8) gives the value at E_{dfe}.

$$J_0(E_{dfe})=\begin{bmatrix} -\mu_h & 0 & 0 & 0 & 0 & \eta^* & 0 & 0 & 0 & -A_4 \\ 0 & -A_7 & 0 & 0 & 0 & 0 & 0 & 0 & 0 & A4 \\ 0 & \epsilon^*\omega^* & -A_1 & 0 & 0 & 0 & 0 & 0 & 0 & 0 \\ 0 & A_{12} & 0 & -A_2 & 0 & 0 & 0 & 0 & 0 & 0 \\ 0 & 0 & \rho_1^* & \rho^*2 & -A_3 & 0 & 0 & 0 & 0 & 0 \\ 0 & 0 & \sigma_1^* & \gamma_1^* & A_8 & -A_9 & 0 & 0 & 0 & 0 \\ 0 & 0 & 0 & 0 & 0 & 0 & -A_{10} & 0 & 0 & -A_6 \\ 0 & 0 & 0 & 0 & 0 & 0 & 0 & -A_{10} & 0 & A_6 \\ 0 & 0 & -\beta_2^*A_5 & -\beta_3^*A_5 & -\beta_4^*A_5 & 0 & 0 & -A_{13} & -A_{11} & 0 \\ 0 & 0 & \beta_2^*A_5 & \beta_3^*A_5 & \beta_4^*A_5 & 0 & 0 & A_{13} & 0 & -A_{11} \end{bmatrix}, \tag{8}$$

where

$$A_4=\frac{\beta_1^*\lambda_1^*(1-\alpha_{h0}^*)}{\mu_h^*N_h},\quad A_5=\frac{\lambda_3^*(1-\alpha_{h0}^*)}{N_h(\alpha_{v0}^*+\mu_v^*)},\quad A_6=\frac{\beta_1^*\lambda_2^*}{(\alpha_{r0}^*+\mu_r^*)N_r},$$

$$A_7=(\omega^*+\mu_h^*),\quad A_8=\gamma_2^*+\sigma_2^*,\quad A_9=\eta^*+\mu_h^*,\quad A_{10}=\alpha_{r0}^*+\mu_r^*,$$

$$A_{11}=\alpha_{v0}^*+\mu_v^*,\quad A_{12}=(1-\epsilon_0^*)\omega^*,\quad A_{13}=\frac{\beta_5^*\lambda_3^*}{N_r(\alpha_{v0}^*+\mu_v^*)}.$$

It is evident that $\mathcal{Z}_1=-\mu_h^*$, $\mathcal{Z}_2=-A_9$, and $\mathcal{Z}_3=-A_{10}$, $\mathcal{Z}_4=-A_{11}$ are the four negative eigenvalues. We take into consideration the following reduced matrix [31] for the remaining eigenvalues:

$$J_1(E_{dfe}) = \begin{bmatrix} -A_7 & 0 & 0 & 0 & 0 & A4 \\ \epsilon^*\omega^* & -A_1 & 0 & 0 & 0 & 0 \\ A_{12} & 0 & -A_2 & 0 & 0 & 0 \\ 0 & \rho_1^* & \rho^*2 & -A_3 & 0 & 0 \\ 0 & 0 & 0 & 0 & -A_{10} & A_6 \\ 0 & \beta_2^* A_5 & \beta_3^* A_5 & \beta_4^* A_5 & A_{13} & -A_{11} \end{bmatrix}.$$

After simplification, we get equation (9):

$$J_1(E_{dfe}) = \begin{bmatrix} -A_7 & 0 & 0 & 0 & 0 & A4 \\ 0 & -A_1A_7 & 0 & 0 & 0 & +\epsilon^*\omega^*A4 \\ 0 & 0 & -A_2A_7 & 0 & 0 & +A_4A_{12} \\ 0 & 0 & 0 & -A_3A_1A_7A_2 & 0 & 0 \\ 0 & 0 & 0 & 0 & -A_{10} & A_6 \\ 0 & 0 & 0 & 0 & 0 & L \end{bmatrix} \tag{9}$$

$L = \frac{\lambda_v^*\beta_1^*\lambda_h^*(1-\alpha_{h0}^*)^2\omega^*\left(A_2A_3\beta_2^*\epsilon_0^*+\beta_4^*\epsilon_0^*\rho_1^*A_2+A_1(1-\epsilon_0^*)(A_3\beta_3^*+\beta_4^*\rho_2^*)\right)}{(\omega^*+\mu_h^*)A_1A_2A_3\mu_h^*N_h^2} + \frac{\lambda_v^*\beta_1^*\beta_5^*\lambda_r^*}{(\mu_r^*+\alpha_{r0}^*)^2N_r^2(\mu_v^*+\alpha_{v0}^*)} - A_{11}$. The eigenvalues of $J_1(E_{dfe})$ take the following form:

$$\mathcal{Z}_5 = -A_7, \quad \mathcal{Z}_6 = -A_1A_7, \quad \mathcal{Z}_7 = -A_2A_7,$$
$$\mathcal{Z}_8 = -A_3A_1A_7A_2, \quad \mathcal{Z}_9 = -A_{10}, \quad \mathcal{Z}_{10} = \frac{\mathcal{R}_0^2}{(\mu_r^*+\alpha_{r0}^*)} - A_{11}.$$

The last eigenvalue also has the negative real part since

$$\frac{\mathcal{R}_0^2}{(\mu_r^*+\alpha_{r0}^*)(\mu_v^*+\alpha_{v0}^*)} < 1,$$

which implies that

$$\frac{\mathcal{R}_0}{\sqrt{(\mu_r^*+\alpha_{r0}^*)(\mu_v^*+\alpha_{v0}^*)}} < 1,$$

implying that $\mathcal{Z}_{10} < 0$, then $\mathcal{R}_0 < 1$, so the system of equation (1) is locally asymptotically stable for $\mathcal{R}_0 < 1$, and implying that

$$\mathcal{R}_0 > \sqrt{(\mu_r^*+\alpha_{r0}^*)(\mu_v^*+\alpha_{v0}^*)},$$

then $\mathcal{Z}_{10} > 0$, we obtain that $\mathcal{R}_0 > 1$, hence the system (1) is unstable for $\mathcal{R}_0 > 1$. □

Data-fitting was used to calculate model (3) parameters and coefficients in Table 1. The Markov Chain Monte Carlo method fitting strategy was used to simulate and evaluate parameters based on eastern Sudan's yearly cumulative VL cases [32,33]. Table 2 summarizes the starting settings for the Fractional VL model.

Table 1 extensively discusses model parameters, including values and ranges. The table displays detection, intervention, transmission, incubation, mortality, treatment, natural recovery, progression, and constant growth and death rates for human, reservoir, and vector populations. Parameter values, calculated or obtained from various sources, are crucial for the model's dynamics.

In Table 2 shows initial value estimations, which are essential to model setup. These statistics represent the initial numbers of susceptible, exposed, undetected infected, PKDL, and immune people, as well as the size of human, reservoir, and vector populations. The table displays the estimated reproduction number R_0, which provides insight into the disease's potential spread.

4.4. Sensitivity analysis

Model (1) was sensitivity analyzed using Latin Hypercube Sampling (LHS) and Partial Rank Correlation Coefficient. This research identifies model dynamics-affecting parameters [40]. LHS stratifies sampling by partitioning each parameter's range of interest into N equidistant intervals and randomly sampled from each. PRCC is helpful for examining nonlinear, monotonic input-output relationships [40]. PRCC findings quantify parameter-outcome relationships. Positive results suggest that raising the parameter improves the outcome, whereas negative results indicate the opposite.

A uniform distribution was assumed for each parameter in θ, 3000 samples were randomly generated, and PRCC results were calculated for the total number of reported cases I_d^* and the basic reproduction number $\mathcal{R}_0$. Fig. 2 displays the analysis findings at a

Table 1
Description of the model parameters.

Par.	Description	Value	Range	Source
$\epsilon(t)$	Average detection rate	0.170	[0.1, 0.5]	Fitted
$\alpha_h^*(t)$	Non-pharmaceutical intervention efficacy	0.70	[0.29, 0.8]	Fitted
$\alpha_r^*(t)$	The effectiveness of initiatives for reservoir control	0.150	[0.01, 0.44]	Fitted
$\alpha_v^*(t)$	Interventional effectiveness in vector control	0.5	[0.13, 1]	Fitted
β_1^*	VL transmission likelihood from Iv to susceptible host	0.560	[0.2212, 0.94]	Fitted
β_2^*	The likelihood of VL transmission from an infected person to Sv	0.340	[0.004, 0.923]	Fitted
β_3^*	Transmission likelihood of VL from Iu to Sv.	0.40	[0.04, 0.93]	Fitted
β_4^*	Probability of VL transmission from Ph to Sv	0.370	[0.02, 0.94]	Fitted
β_5^*	VL transmission likelihood from Ir to Sv	0.74	[0.3, 0.97]	Fitted
$\frac{1}{\omega^*}$	Human average VL incubation time	60 days	[30, 180]	[34,35]
δ_1^*	VL-induced mortality rate in Id group	4.015	TBD	[23,35]
δ_2^*	VL-induced mortality rate in Iu group	4.015	TBD	[23,35]
δ_3^*	Treatment rate for Ph group	4.015	TBD	[23,35]
σ_1^*	Treatment rate for Id group I_d class	0.030 day^{-1}	-	[23]
σ_2^*	Treatment rate for Ph group	0.0330 day^{-1}	-	[36]
γ_1^*	Rate of natural recovery for Iu class	0.840	[0.8, 0.9]	[23]
γ_2^*	rate of natural recovery for Ph group	0.005 day^{-1}	[0.001, 0.005]	[23]
ρ_1^*	Rate of progression from Id class to Ph group	0.360	-	[36]
ρ_2^*	Rate of Iu class to Ph class progression	0.0001	[0.0001, 0.0002]	[23]
η^*	Rate of progression from Rh to Sh group	0.002 day^{-1}	[0.001, 0.006]	[23]
λ_h^*	Constant population growth	0.0270	-	[37]
λ_r^*	Constant Population growth in reservoirs	$\mu_h^* \times N_r(0)$	-	[23,38]
λ_v^*	Constant rate of growth of the Nv	$\mu_h^* \times N_v(0)$	-	[23,38]
μ_h^*	Constant death rate of human population	0.00670	-	[37]
μ_r^*	Constant death rate of human reservoir	0.00170 day^{-1}	-	[39]
μ_v^*	Constant death rate of vector population	0.06680 day^{-1}	-	[23]

Table 2
Descriptions for the initial values.

Par.	Description	Formula	Range (95% CI)
$N_h^*(0)$	Initial size of N_h^*	0.10859×10^7	$[1.0084, 1.37] \times 10^6$
$S_h^*(0)$	Initial size of S_h^*	$0.27 \times N_h^*(0)$	$[0.01, 0.87] \times N_h^*(0)$
$E_h^*(0)$	Initial size of E_h^*	$0.210 \times S_h^*(0)$	$[0.01, 0.9] \times S_h^*(0)$
$I_u^*(0)$	Initial size of I_u^*	$0.36590 \times E_h^*(0)$	$[0.08, 0.9] \times E_h^*(0)$
$P_h^*(0)$	Initial size of P_h^*	$0.3659 \times [I_d^*(0) + I_u^*(0)]$	[0.08, 0.93]
$R_h^*(0)$	Initial size of R_h^* *	TBE	
$N_r^*(0)$	Initial size of N_r^*	$0.180 \times N_h^*(0)$	$[0.1, 0.3] \times N_h^*(0)$
$I_r^*(0)$	Initial size of I_r^*	$0.070 \times N_r^*(0)$	$[0.02, 0.3] \times N_r^*(0)$
$N_v^*(0)$	Initial size of N_v^*	$6.150 \times N_h^*(0)$	$[2.14, 9.3] \times N_h^*(0)$
$I_v^*(0)$	Initial size of infected vector population	$0.2 \times N_v^*(0)$	$[0.05, 0.54] \times N_v^*(0)$
R_0	Estimated reproduction number	8.040	[6.41, 9.03]

95% confidence level for each input parameter. According to Fig. 2 **A**, ϵ^*, β_1^*, β_5^*, N_v^*, S_h^* have a substantial positive impact on I_d^*, while α_h^* and N_r^* have a considerable negative impact. ϵ^* has the greatest beneficial impact on I_d^* see Table 3), as higher reporting rates lead to more cases being recognized. The most significant negative impact on I_d^* is from α_h^* see Table 3), indicating that greater human population protection efforts lead to fewer community cases.

However, only a small number of parameters have a considerable impact on the value of $\mathcal{R}_0$ (see to Fig. 2 **B**). These parameters include $\beta_1^*, N_v, \alpha_r^*, \alpha_v^*$, and N_r^*. It is interesting to note that we discovered two discoveries that are consistent with the findings of those of other studies: There is a significant correlation between an increase in β_1^*, which represents the interaction rate between sand-flies and hosts (humans and reservoirs), and an increase in the basic reproduction number $\mathcal{R}_0$ [35]. Additionally, a decrease in N_r, which represents the total size of the reservoir population, can lead to an increase in the number of cases of VL among the human population [41,42].

5. Numerical simulations

Our fractional-order model's dynamics were successfully simulated using the Fractional Euler Method see [43], and we present a graphical numerical solution of our proposed model in the sense of the Caputo fractional derivative for a value of $\alpha = 1, 0.99, 0.98, 0.97$ and 0.96. Using the Caputo operator, various fractional-order values were used to depict numerical simulations of susceptible, exposed, infected, and recovered individuals. MATLAB was used to run all numerical simulations in this investigation, using the initial and parameter values listed in Table 1 and Table 2, respectively. Data were collected by the Sudanese Ministry of Health in Gedaref State, Eastern Sudan.

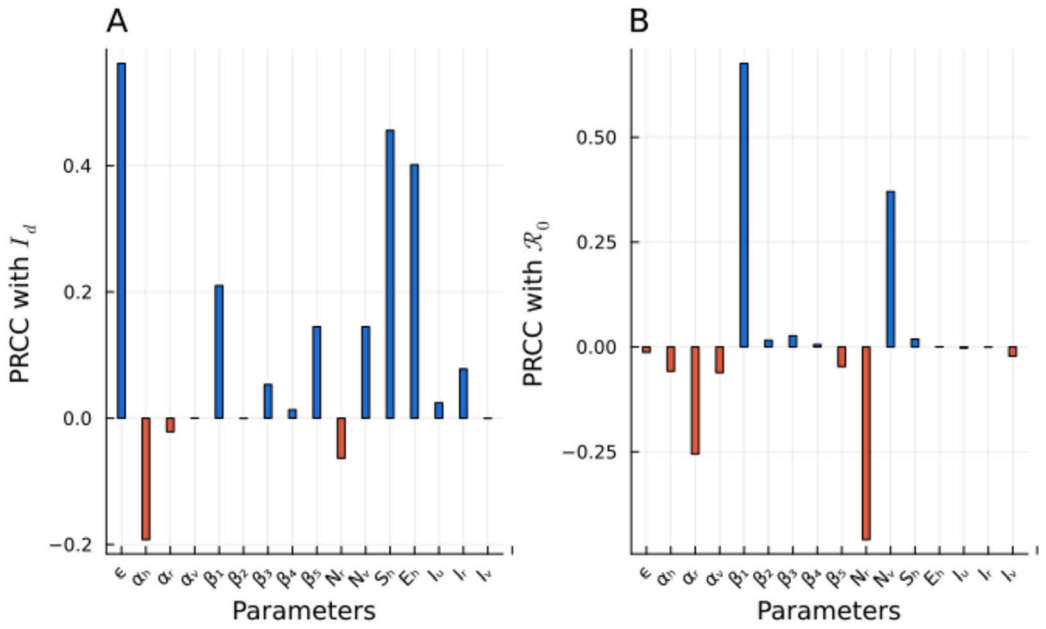

Fig. 2. shows PRCC findings for model parameters, including I_d **(A)** and $\mathcal{R}_0$ **(B)**. The bars' height represents correction intensity, with blue indicating positive correlation and red indicating negative correlation.

Table 3
Partial rank correlation coefficient r and p-value of each parameter with both I_d^* and $\mathcal{R}_0$.

	PRCC with I_d		PRCC with $\mathcal{R}_0$	
Parameter	r	p-value	r	p-value
ϵ^*	56.2e−2	15.9e−4	−1.29e−2	0.214
α_h^*	−0.192	0.000283	−0.0579	0.000961
α_r^*	−0.0213	0.427	−0.255	0
α_v^*	0.00033	0.145	−0.0613	0.00153
β_1^*	0.21	6.27e−8	0.676	0
β_2^*	−0.000256	0.0636	0.0159	0.178
β_3^*	0.0533	0.466	0.0266	0.0316
β_4^*	0.0134	0.73	0.00571	0.219
β_5^*	14.5e−2	0.0202e−3	−0.047	0.0.113e−2
N_r	−6.32e−2	0.184e−8	−0.459	0
N_v	0.145	8.98e−6	0.37	0
S_h	0.456	0.0159	0.0187	0.44
E_h	0.401	0.577	0.000359	0.877
I_u	2.45e−2	32.3e−2	−0.00276	0.874
I_r	7.81e−2	2.51e−2	−0.00067	0.168
I_v	−0.000326	0.954	−0.0222	0.143

To examine the approximate solutions for the Susceptible, Exposed, detected, and undetected infected individuals within the human population, as well as the Susceptible and Infected vectors and Susceptible and Infected reservoirs, our proposed model is presented. Figs. 3 and 4 visually depicts these solutions, which represent the overall population size for each category (Susceptible, Exposed, Detected Infected, and undetected infected) over time (t). The aforementioned figures have been derived based on a variety of fractional-order values. Fig. 3 illustrates the population size of individuals who are susceptible to a particular condition, revealing a gradual decline over a span of two decades. According to Fig. 3, there is an anticipated upward trend in the number of exposed cases during the specified time frame. The number of detected infected cases is depicted in Fig. 4, indicating an anticipated increase in the future. The projected increase in the number of undetected infected individuals is anticipated to occur gradually, as depicted in Fig. 4. Additionally, it can be observed from Fig. 5 that there is a simultaneous decline in the population of susceptible and infected vectors during the given time frame. Ultimately, it is anticipated that the Susceptible and Infected reservoirs will exhibit a decline in magnitude as time progresses, as visually depicted in Fig. 6.

Furthermore, the computations of absolute and relative errors for various fractional orders are included in Table 4 within the table.

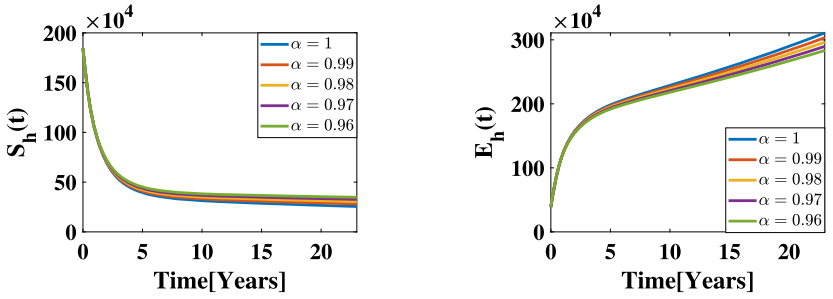

Fig. 3. The state variables $S_h^*(t)$ and $E_h^*(t)$ for different fractional orders.

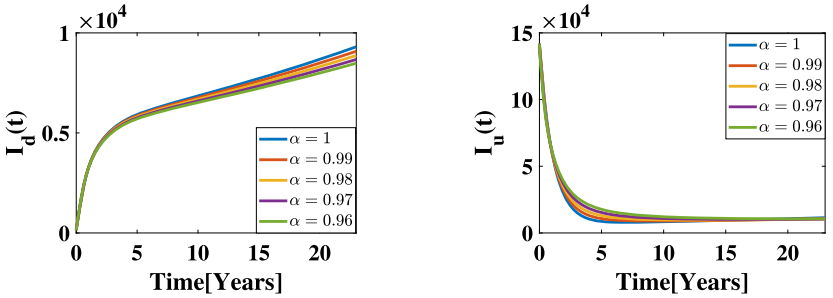

Fig. 4. The state variables $I_d^*(t)$ and $I_u^*(t)$ for different fractional orders.

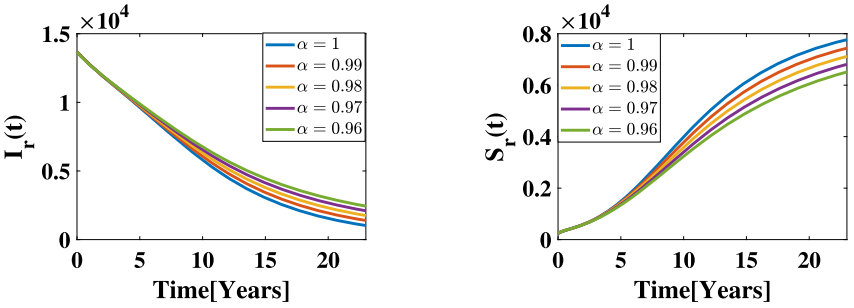

Fig. 5. The state variables $I_r^*(t)$ and $S_r^*(t)$ for different fractional orders.

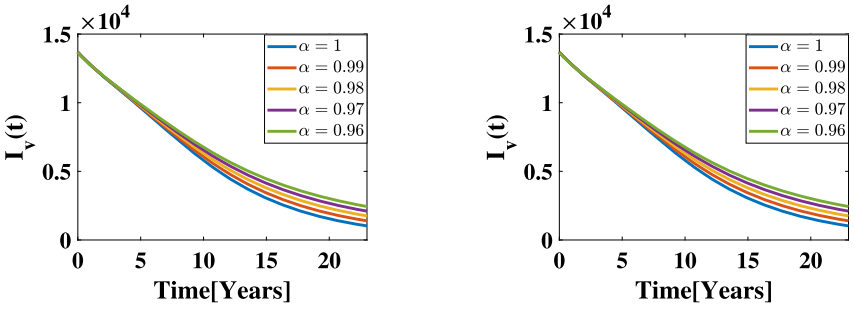

Fig. 6. The state variables $I_v^*(t)$ and $S_v^*(t)$ for different fractional orders.

The comparison findings from the error analysis presented in Table 4 indicate that the curves exhibit higher levels of accuracy when the non-integer order α is set to 0.99. Notably, the fractional response with $\alpha = 0.99$ demonstrates superior precision compared to the classical response with $\alpha = 1$.

The aforementioned advantages can be attributed to the inherent flexibility of the fractional model, which allows for the adaptation of its fractional order to effectively capture real-world data. So, the results shown in Fig. 7 and Table 4 show that a fractional

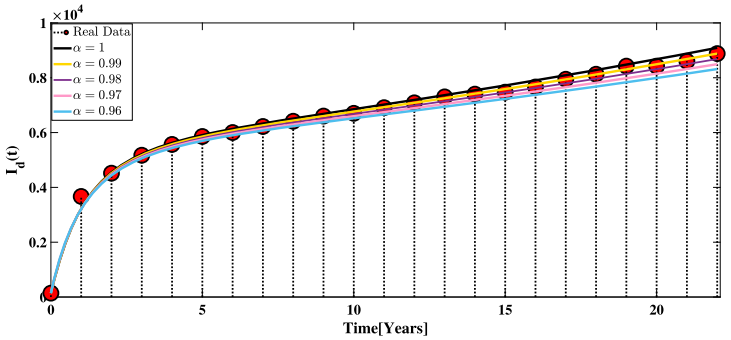

Fig. 7. Simulation results versus real data.

Table 4
Absolute and relative errors for different fractional orders.

Fractional-order	Absolute error	Relative error
0.96	6.3774×10^3	0.92217
0.97	4.3394×10^3	0.64501
0.98	2.2419×10^3	0.3613
0.99	1.2769×10^3	0.23471
1	3.2468×10^3	0.50423

calculus modeling approach, instead of the current integer-order scheme, is more likely to accurately represent what happens in the real world.

It is worth noting that the computational cost of the fractional-order models will be more expensive than the integer-order models, but some fast and parallel method like [44,45] can be used to reduce the computational complexity well, so it is not a serious problem and furthermore this fact can be attributed to the increased flexibility offered by fractional models.

6. Conclusion

In this study, the primary innovation lies in the application of the Caputo fractional derivative to model the dynamics of disease spread. This approach allows us to capture more complex behaviors of the system, such as memory effects, which are not possible with standard derivatives. By focusing on local stability around the disease-free equilibrium, we've provided essential insights into the initial stages of disease outbreaks, which are crucial for immediate public health interventions. This is contextualized through the calculation of the basic reproduction number R_0, a key parameter in epidemiological studies. While the paper does not delve into global stability or multiple steady states, it lays the groundwork for such analyses in future research. The model is designed to be extensible, allowing other researchers to build upon it to explore these and other complexities specially in new models with fractional derivatives such as [46] and [47]. The manuscript aims to strike a balance between mathematical rigor and practical applicability. By introducing a fractional-order model in the context of disease spread, we hope to inspire further interdisciplinary work that brings complex systems theory into public health.

Ethics statement

This research employs a thorough modeling analysis of de-identified data on leishmaniasis statistics gathered by the Health Information Centre, Ministry of Health, Gedaref State, Sudan. Therefore, this study activity does not need ethical examination and approval.

CRediT authorship contribution statement

Rania Saadeh: Writing – review & editing, Writing – original draft, Visualization, Validation, Supervision, Software, Resources, Project administration, Methodology, Investigation, Funding acquisition, Formal analysis, Data curation, Conceptualization. **Mohamed A. Abdoon:** Writing – review & editing, Writing – original draft, Visualization, Validation, Supervision, Software, Resources, Project administration, Methodology, Investigation, Funding acquisition, Formal analysis, Data curation, Conceptualization. **Ahmad Qazza:** Writing – review & editing, Writing – original draft, Visualization, Validation, Supervision, Software, Resources, Project administration, Methodology, Investigation, Funding acquisition, Formal analysis, Data curation, Conceptualization. **Mohammed Berir:** Methodology, Investigation, Funding acquisition, Formal analysis, Data curation, Conceptualization. **Fathelrhman EL Guma:** Methodology, Investigation, Funding acquisition, Formal analysis, Data curation, Conceptualization. **Naseam Al-kuleab:** Methodol-

ogy, Investigation, Funding acquisition, Formal analysis, Data curation, Conceptualization. **Abdoelnaser M Degoot:** Methodology, Investigation, Funding acquisition, Formal analysis, Data curation, Conceptualization.

Declaration of competing interest

The authors of this manuscript declare no conflict of interests.

Data availability

The data are available from the corresponding authors upon request.

References

[1] M.A. Abdoon, R. Saadeh, M. Berir, F.E. Guma, et al., Analysis, modeling and simulation of a fractional-order influenza model, Alex. Eng. J. 74 (2023) 231–240.
[2] A. Qazza, M. Abdoon, R. Saadeh, M. Berir, A new scheme for solving a fractional differential equation and a chaotic system, Eur. J. Pure Appl. Math. 16 (2) (2023) 1128–1139.
[3] R. Saadeh, M. Abdoon, A. Qazza, M. Berir, A numerical solution of generalized Caputo fractional initial value problems, Fractal Fract. 7 (4) (2023) 332.
[4] A. Qazza, R. Saadeh, O. Ala'yed, A. El-Ajou, Effective transform-expansions algorithm for solving non-linear fractional multi-pantograph system, AIMS Math. 8 (9) (2023) 19950–19970.
[5] R. Lainson, J.J. Shaw, et al., Evolution, Classification and Geographical Distribution, Academic Press, 1987.
[6] E. Zijlstra, M.S. Ali, A. El-Hassan, I.A. El Toum, M. Satti, H. Ghalib, P. Kager, Direct agglutination test for diagnosis and sero-epidemiological survey of kala-azar in the Sudan, Trans. R. Soc. Trop. Med. Hyg. 85 (4) (1991) 474–476.
[7] R. Reithinger, R.J. Quinnell, B. Alexander, C.R. Davies, Rapid detection of leishmania infantum infection in dogs: comparative study using an immunochromatographic dipstick test, enzyme-linked immunosorbent assay, and PCR, J. Clin. Microbiol. 40 (7) (2002) 2352–2356.
[8] M. Marlet, F. Wuillaume, D. Jacquet, K. Quispe, J. Dujardin, M. Boelaert, A neglected disease of humans: a new focus of visceral leishmaniasis in Bakool, Somalia, Trans. R. Soc. Trop. Med. Hyg. 97 (6) (2003) 667–671.
[9] J. Alvar, P. Aparicio, A. Aseffa, M. Den Boer, C. Canavate, J.-P. Dedet, L. Gradoni, R. Ter Horst, R. López-Vélez, J. Moreno, The relationship between leishmaniasis and aids: the second 10 years, Clin. Microbiol. Rev. 21 (2) (2008) 334–359.
[10] P. De Beer, A. El Harith, L. Deng, S. Semiao-Santos, B. Chantal, M. van Grootheest, A killing disease epidemic among displaced Sudanese population identified as visceral leishmaniasis, Am. J. Trop. Med. Hyg. 44 (3) (1991) 283–289.
[11] V.V. Albani, J.P. Zubelli, Stochastic transmission in epidemiological models, J. Math. Biol. 88 (3) (2024), https://doi.org/10.1007/s00285-023-02042-z.
[12] I. Ghosh, T. Sardar, J. Chattopadhyay, A mathematical study to control visceral leishmaniasis: an application to South Sudan, Bull. Math. Biol. 79 (5) (2017) 1100–1134.
[13] Y. Song, T. Zhang, H. Li, K. Wang, X. Lu, Mathematical model analysis and simulation of visceral leishmaniasis, Kashgar, Xinjiang, 2004–2016, Complexity 2020 (2020) 1–14.
[14] I.M. ELmojtaba, Mathematical model for the dynamics of visceral leishmaniasis–malaria co-infection, Math. Methods Appl. Sci. 39 (15) (2016) 4334–4353.
[15] M. Sinan, K.J. Ansari, A. Kanwal, K. Shah, T. Abdeljawad, B. Abdalla, et al., Analysis of the mathematical model of cutaneous leishmaniasis disease, Alex. Eng. J. 72 (2023) 117–134.
[16] T.-Q. Tang, R. Jan, H. Ahmad, Z. Shah, N. Vrinceanu, M. Racheriu, A fractional perspective on the dynamics of hiv, considering the interaction of viruses and immune system with the effect of antiretroviral therapy, J. Nonlinear Math. Phys. (2023) 1–18.
[17] M. Farhan, Z. Shah, R. Jan, S. Islam, A fractional modeling approach of Buruli ulcer in Possum mammals, Phys. Scr. 98 (6) (2023) 065219.
[18] T.-Q. Tang, Z.U. Rehman, Z. Shah, R. Jan, N. Vrinceanu, M. Racheriu, Modeling and analysis of the transmission of avian spirochetosis with non-singular and non-local kernel, Comput. Methods Biomech. Biomed. Eng. (2023) 1–13.
[19] Y.-M. Chu, M.F. Khan, S. Ullah, S.A.A. Shah, M. Farooq, M. bin Mamat, Mathematical assessment of a fractional-order vector–host disease model with the Caputo–Fabrizio derivative, Math. Methods Appl. Sci. 46 (1) (2023) 232–247.
[20] S. Uçar, Analysis of hepatitis B disease with fractal–fractional Caputo derivative using real data from Turkey, J. Comput. Appl. Math. 419 (2023) 114692.
[21] M. Vellappandi, P. Kumar, V. Govindaraj, W. Albalawi, An optimal control problem for mosaic disease via Caputo fractional derivative, Alex. Eng. J. 61 (10) (2022) 8027–8037.
[22] K. Shah, A. Khan, B. Abdalla, K.A. Khan, T. Abdeljawad, A mathematical model for Nipah virus disease by using piecewise fractional order Caputo derivative, Fractals (2023).
[23] A. Stauch, R.R. Sarkar, A. Picado, B. Ostyn, S. Sundar, S. Rijal, M. Boelaert, J.-C. Dujardin, H.-P. Duerr, Visceral leishmaniasis in the Indian subcontinent: modelling epidemiology and control, PLoS Negl. Trop. Dis. 5 (11) (2011) e1405.
[24] P. Van den Driessche, J. Watmough, Reproduction numbers and sub-threshold endemic equilibria for compartmental models of disease transmission, Math. Biosci. 180 (1–2) (2002) 29–48.
[25] I. Podlubny, Fractional Differential Equations: an Introduction to Fractional Derivatives, Fractional Differential Equations, to Methods of Their Solution and Some of Their Applications, Elsevier, 1998.
[26] D. Baleanu, S. Arshad, A. Jajarmi, W. Shokat, F.A. Ghassabzade, M. Wali, Dynamical behaviours and stability analysis of a generalized fractional model with a real case study, J. Adv. Res. 48 (2023) 157–173.
[27] F.E. Guma, O.M. Badawy, M. Berir, M.A. Abdoon, Numerical analysis of fractional-order dynamic Dengue disease epidemic in Sudan, J. Niger. Soc. Phys. Sci. 5 (2) (2023) 1464, pp. 1–6.
[28] C. Milici, G. Drăgănescu, J.T. Machado, Introduction to Fractional Differential Equations, vol. 25, Springer, 2018.
[29] H. Smith, P. Waltman, The Theory of the Chemostat: Dynamics of Microbial Competition, Cambridge University Press, 1995.
[30] M. Ali, M. Bakheet, E. Bashier, A mathematical model for non-pharmaceutical interventions in the transmission of Covid-19, J. Math. Comput. Sci. 12 (2022).
[31] K. Khan, R. Zarin, A. Khan, A. Yusuf, M. Al-Shomrani, A. Ullah, Stability analysis of five-grade leishmania epidemic model with harmonic mean-type incidence rate, Adv. Differ. Equ. 2021 (2021) 86.
[32] A. Endo, E. Van Leeuwen, M. Baguelin, Introduction to particle Markov-chain Monte Carlo for disease dynamics modellers, Epidemics 29 (2019) 100363.
[33] T.K. Martheswaran, H. Hamdi, A. Al-Barty, A.A. Zaid, B. Das, Prediction of Dengue fever outbreaks using climate variability and Markov chain Monte Carlo techniques in a stochastic susceptible-infected-removed model, Sci. Rep. 12 (1) (2022) 5459.
[34] S. Zhao, Y. Kuang, C.-H. Wu, D. Ben-Arieh, M. Ramalho-Ortigao, K. Bi, Zoonotic visceral leishmaniasis transmission: modeling, backward bifurcation, and optimal control, J. Math. Biol. 73 (2016) 1525–1560.
[35] Y. Song, T. Zhang, H. Li, K. Wang, X. Lu, Mathematical model analysis and simulation of visceral leishmaniasis, Kashgar, Xinjiang, 2004–2016, Complexity 2020 (2020) 1–14.

[36] S. Gasim, A. Elhassan, A. Kharazmi, E. Khalil, A. Ismail, T. Theander, The development of post-kala-azar dermal leishmaniasis (PKDL) is associated with acquisition of leishmania reactivity by peripheral blood mononuclear cells (PBMC), Clin. Exp. Immunol. 119 (3) (2000) 523–529.
[37] T.W. Bank, Sudan data, data retrieved from World Development Indicators, https://data.worldbank.org/country/sudan, 2023.
[38] S. Biswas, A. Subramanian, I.M. ELMojtaba, J. Chattopadhyay, R.R. Sarkar, Optimal combinations of control strategies and cost-effective analysis for visceral leishmaniasis disease transmission, PLoS ONE 12 (2) (2017) e0172465.
[39] C. Dye, The logic of visceral leishmaniasis control, Am. J. Trop. Med. Hyg. 55 (2) (1996) 125–130.
[40] S. Marino, I.B. Hogue, C.J. Ray, D.E. Kirschner, A methodology for performing global uncertainty and sensitivity analysis in systems biology, J. Theor. Biol. 254 (1) (2008) 178–196.
[41] I.M. ELmojtaba, J. Mugisha, M.H. Hashim, Mathematical analysis of the dynamics of visceral leishmaniasis in the Sudan, Appl. Math. Comput. 217 (6) (2010) 2567–2578.
[42] L.F. Chaves, M.-J. Hernandez, A.P. Dobson, M. Pascual, Sources and sinks: revisiting the criteria for identifying reservoirs for American cutaneous leishmaniasis, Trends Parasitol. 23 (7) (2007) 311–316.
[43] A.A. Kilbas, M. Saigo, R.K. Saxena, Generalized Mittag-Leffler function and generalized fractional calculus operators, Integral Transforms Spec. Funct. 15 (1) (2004) 31–49.
[44] X.-M. Gu, S.-L. Wu, A parallel-in-time iterative algorithm for Volterra partial integro-differential problems with weakly singular kernel, J. Comput. Phys. 417 (2020) 109576.
[45] S. Jiang, J. Zhang, Q. Zhang, Z. Zhang, Fast evaluation of the Caputo fractional derivative and its applications to fractional diffusion equations, Commun. Comput. Phys. 21 (3) (2017) 650–678.
[46] X.M. Gu, H.W. Sun, Y.L. Zhao, X. Zheng, An implicit difference scheme for time-fractional diffusion equations with a time-invariant type variable order, Appl. Math. Lett. 120 (2021) 107270.
[47] X.-M. Gu, T.-Z. Huang, Y.-L. Zhao, P. Lyu, B. Carpentieri, A fast implicit difference scheme for solving the generalized time–space fractional diffusion equations with variable coefficients, Numer. Methods Partial Differ. Equ. 37 (2) (2021) 1136–1162.